Supporting information for

Moisture absorbent gel electrolyte enables aqueous and flexible supercapacitor operated at high temperatures

Lingyang Liu,[a,b] Qingyun Dou,[a,b] Yinglun Sun,[a,b] Yulan Lu,[a,c] Qingnuan Zhang,[a] Jianing Meng,[a,d] Xu Zhang,[a] Siqi Shi,[e] Xingbin Yan [a,b,f,*]

a. Laboratory of Clean Energy Chemistry and Materials, State Key Laboratory of Solid Lubrication, Lanzhou Institute of Chemical Physics, Chinese Academy of Sciences, Lanzhou 730000, P. R. China. E-mail: xbyan@licp.cas.cn

b. Center of Materials Science and Optoelectronics Engineering, University of Chinese Academy of Sciences, Beijing 100080, P. R. China.

c. School of Physical Science and Technology, Lanzhou University, Lanzhou 730000, P. R. China.

d. Cuiying Honors College, Lanzhou University, Lanzhou 730000, P. R. China.

e. School of Materials Science and Engineering, Shanghai University, Shanghai 200444, P. R. China.

f. Dalian National Laboratory for Clean Energy, Dalian Institute of Chemical Physics, Chinese Academy of Sciences, Dalian 116000, P. R. China.

Corresponding Author

* E-mail: xbyan@licp.cas.cn

Table S1. Mass contents (wt.%) of the components in 1M LiCl-PVA and 21m LiTFSI-PVA gels.

	1M LiCl-PVA gel	21m LiTFSI-PVA gel
PVA	8.75%	5.38%
H_2O	87.54%	13.46%
Li salt	3.71%	81.16%

Table S2. The mass retention rates of 1M LiCl-PVA and 21m LiTFSI-PVA gels under different conditions.

Temperature and humidity	Time (h)	Mass retention rate	
		1M LiCl-PVA	21m LiTFSI-PVA
environmental condition	100	63.2%	113%
80 °C-50% RH	12	14.5%	118%
100 °C-50% RH	8	22.3%	118%
100 °C-10% RH	7	17.1%	104%
120 °C	3.2	22.4%	98.1%
150 °C	1.5	23.3%	94.1%

Table S3. The capacitance retention rates of 1M LiCl-PVA and 21m LiTFSI-PVA gels under different conditions.

Temperature and humidity	1M LiCl-PVA		21m LiTFSI-PVA	
	Cycle time (h)	Capacitance retention rate	Cycle time (h)	Capacitance retention rate
environmental condition	20	almost 0%	1500 (62 days)	98.8%
80 °C-50 % RH	0.5	0%	100	80.8%
100 °C-10 % RH	-	-	44.1	80.1%
120 °C	-	-	12.5	79.3%

Table S4. Comparison of the high temperature performance with the reported state-of-the-art aqueous supercapacitors.

Electrode	Electrolyte	Voltage	High temperature	Cycle time	references
Carbon cloth	21m LiTFSI-PVA gel	1.8 V	80 °C	100 h	Our work
			100 °C	44.1	
			120 °C	12.5	
PEDOTS-RuO_2@PEDOTS	LiCl-PVA	1.5 V	75 °C	~15 h	24
Ni-Co MOF//AC	6M KOH-PBI	1.8 V	50 °C	X	25
MnO_2//Graphene	H_3PO_4/PVA	1.4 V	80 °C	X	26
Graphene	Li_2SO_4/ethylene glycol/water	1.0 V	45 °C	~22.5 h	27
RuO_2	H_2SO_4	1.2 V	40 °C	X	48
Co_9S_8	KOH	0.6 V	70 °C	X	49
$NiCo_2O_4$	KOH	0.6 V	60 °C	X	50

* The cycle time in other reported papers is concluded with the ~80% capacitance retention rate.

** X means that the cycle was not performed in these papers.

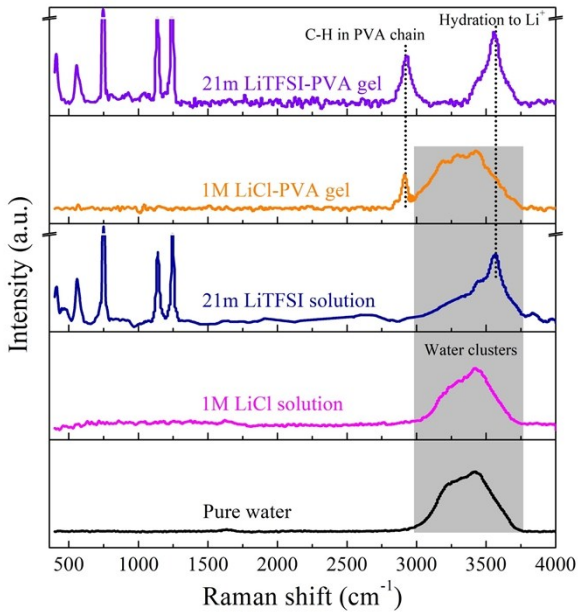

Figure S1. Full Raman spectra of pure water, 1M LiCl solution, 21m LiTFSI solution, 1M LiCl-PVA and 21m LiTFSI-PVA gels.

Note 1. Raoult's law and vapor pressure

From a thermodynamic point of view, highly water-soluble substances have a large water absorption capability (deliquescent tendency), and this is because the concentrated solution has a lower vapor pressure. At 25 °C, the vapor pressure of pure water is 3.12 kPa, and if the vapor pressure of water in a saturated salt solution is lower than the pressure of water vapor in the environment, the solution will absorb water from the environment. The saturated vapor pressure of the same substance increases as the temperature increases.

According to Raoult's law, if the solute is non-volatile, and at a certain temperature, the vapor pressure of the dilute electrolyte solution is equal to the saturated vapor pressure of the pure solvent multiplied by the mole fraction of the solvent.

$$p = p^* \times n_A/(n_A + n_B)$$

where p is the vapor pressure of the dilute electrolyte solution, p^* is the saturated vapor pressure of the solvent, n_A and n_B is the molar weight of solvent and solute.

For the ideal dilute solution, the mutual attraction of solvent and solute does not change during mixing, so the volume change before and after mixing is not large. However, when a typical negative deviation solution whose vapor pressure is less than the calculated value of Raoul's law is formed, the volume shrinks and there is an exothermic phenomenon, indicating a lager interaction between the two types of molecules, which hinders the evaporation of liquid molecules. Another typical feature of this solution is that the two components have a tendency to form a compound.

Since the mole fraction of water in the 21m LiTFSI "water-in-salt" (WIS) solution is very low, the vapor pressure is very low. Moreover, the highly concentrated 21m LiTFSI WIS electrolytes have typical negative-bias properties, including a reduction in total volume and tendency to form compounds when the solvent (water) and solute (LiTFSI) are mixed (which can be seen from preparation process and Raman results of WIS solution). [S1-S6] Therefore, according to the aforementioned description, it can be known that the WIS solution has a much lower saturated vapor pressure than the theoretical value. This value has a larger difference with the vapor pressure in the environment, indicating that it is easier to absorb moisture or retain moisture, and perhaps to avoid evaporation of water in a high temperature environment.

Note 2. activity coefficient, ionic strength and Debye-Hückel theory

The concentration at which the ions actually act in the electrolyte solution is called the

effective concentration, that is, the activity. The correction factor (γ_A) in the modified Raoult's law is called the activity coefficient.

$$p = p^* \times \gamma_A \times n_A/(n_A + n_B)$$

The stronger the interaction between the ions in the solution is, the larger the ionic strength and the smaller the activity coefficient are. Therefore, according to the modified Raoult's law, once the ionic strength of the ions in the solution is large, it means that the vapor pressure of the solution is correspondingly lowered. For ideal dilute solutions, the water activity can be approximated as the ratio of the water vapor pressure of the solution to the saturated vapor pressure of the pure water at the same temperature.

The relationship between ionic strength and ionic activity can be obtained according to the Debye-Hückel formula.

$$\lg \gamma_i = -A \times z_i 2\sqrt{I}$$

where A is a constant factor (at 298 K, the A value of the aqueous solution is 0.509), z_i represents the charge of positive and negative ions and I is ionic strength.

However, this formula is only suitable for ideal solutions with very low concentrations (< 0.02 mol kg^{-1}). In 1961, Davies further modified the formula to accommodate higher ionic strength electrolyte solutions.

$$lg\gamma_i = -0.509 \times |z_+ \times z_-| \times \left(\frac{\sqrt{I}}{1+\sqrt{I}} - 0.30 \times I\right)$$

For solutions with only one salt, the ionic strength can be calculated according to the following formula:

$$I = \frac{1}{2}\sum b_i z_i^2$$

where b_i is the molar weight of anions or cations.

Although these formulas are still not suitable for WIS solution, we can qualitatively understand the difference in ionic activity coefficient or ionic strength of WIS solutions from conventional solutions. After calculation, the activity coefficient of Li^+ ions in 1M LiCl solution is 0.79, and the Li^+ ions activity coefficient in 21m LiTFSI solution is as high as 615. Such a large ionic activity coefficient is normal for solutions with high concentrations, and indicates that the combination of ions and water molecules in solution also has the essential difference which cannot be explained by the conventional Debye-Hückel theory (based on ideal dilute solutions).

Stokes and Robinson found that with the concentration increased, the hydration between ions and water molecules also increases. They believe that strong hydration makes some water molecules look more like solute than solvent, so it is necessary to distinguish the "bound" water molecules and "free" water molecules inside and outside the hydration shells. Based on the aforementioned discussions, they modified Debye-Hückel equation with a "solvent term" (*-(n/v)log* a_w):

$$\lg \gamma_i = -\frac{A\sqrt{I}}{1 + Br\sqrt{I}} - \frac{n}{v} lg a_w - lg(1 - 0.018(n - v)m)$$

where A and B are constants, r is the mean distance of the closest ions, n is the hydration number, v is the number of ions formed by one solute, a_w is the water activity, and m is the molality.

Through this modified equation, we can qualitatively know that an increase in ionic strength leads to a decrease in water activity. Since the ion activity in the WIS solution

is extremely large, its water activity becomes very low. As mentioned above, for ideal dilute solutions, the water activity can be approximated as the ratio of the water vapor pressure of the solution to the saturated vapor pressure of the pure water at the same temperature. That is to say, the water vapor pressure of the concentrated solution is further lower when the saturated vapor pressure of the pure water multiply by a low water activity and mole fraction. These results, in turn, further indicate that the vapor pressure of the WIS solution is ultra-low, which is consistent with the results obtained in other literatures.[S2] Therefore, the ultra-low vapor pressure of the WIS solution ensures strong water retention and water absorption characteristics, and can avoid evaporation of water even in high temperature environments.

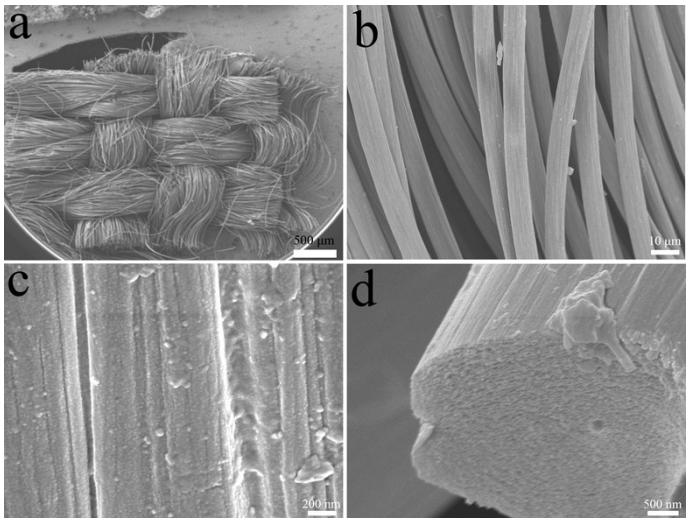

Figure S2. Field-emission scanning electron microscopy (FE-SEM) images of carbon cloth with different magnifications.

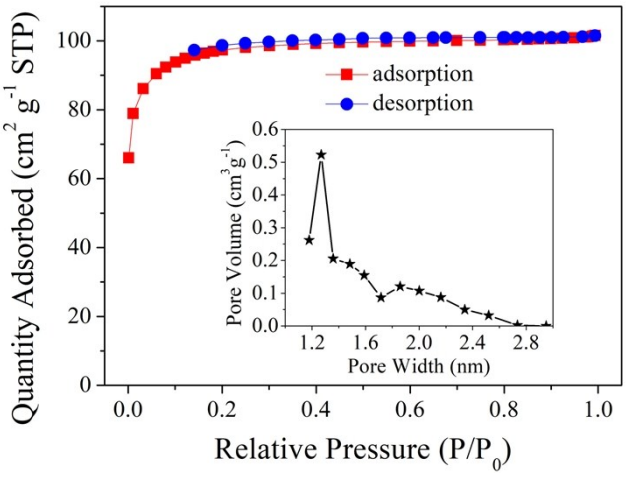

Figure S3. Nitrogen adsorption-desorption isotherm curve and the corresponding pore size distribution (inset) of carbon cloth.

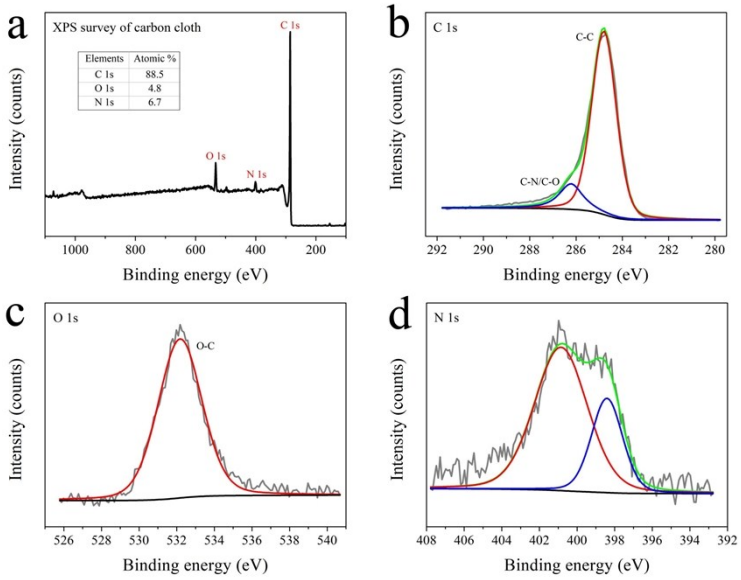

Figure S4. XPS analyses of carbon cloth: (a) XPS survey, insert showing the atomic percentage of C, O and N elements; (b) C 1s, (c) O 1s and (d) N 1s spectra.

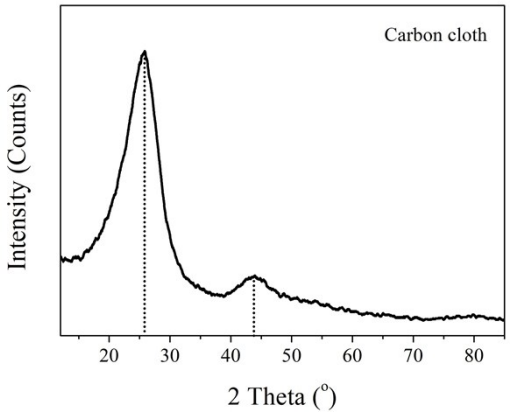

Figure S5. XRD pattern of carbon cloth.

Field-emission scanning electron microscope (FE-SEM) images in Figure S2 shows the microtopography of carbon cloth. The rough surface facilitates the adsorption and desorption of electrolyte ions, further making the carbon cloth a very high specific capacitance. The nitrogen adsorption-desorption curve in Figure S3 indicates that the carbon cloth has a specific surface area of 330.8 m^2 g^{-1}, and it can be seen from the pore size distribution that most are micropores larger than 1 nm, which is very suitable for efficient charge storage of supercapacitors. XPS spectra in Figure S4 and XRD pattern in Figure S5 confirmed the elemental composition and crystallinity of carbon cloth.

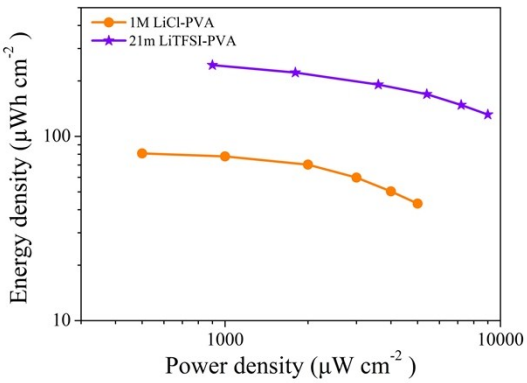

Figure S6. Ragone plots of the quasi-solid-state SCs using 1 M LiCl-PVA and 21 m LiTFSI-PVA gel electrolytes.

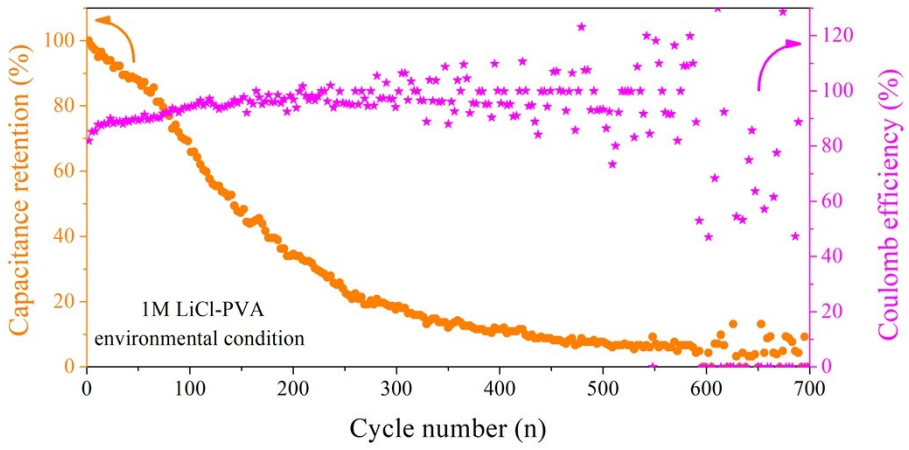

Figure S7. cycle number dependent cycle performance of 1M LiCl-PVA gel electrolyte based supercapacitors under environmental condition.

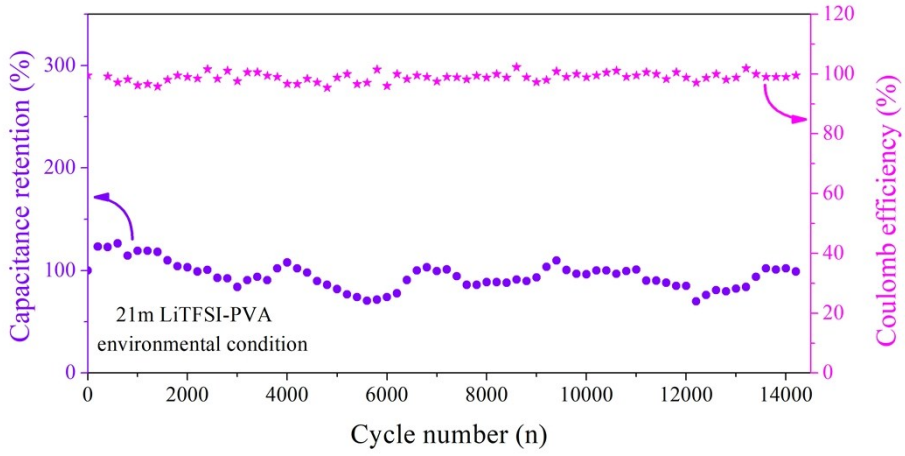

Figure S8. cycle number dependent cycle performance of 21 LiTFSI-PVA gel electrolyte based supercapacitors under environmental condition.

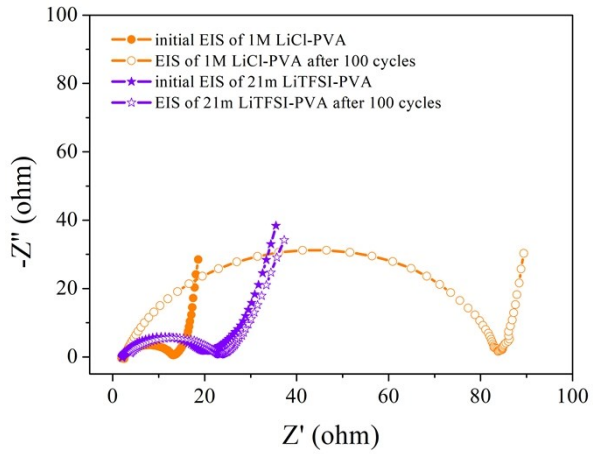

Figure S9. EIS plots of 1M LiCl-PVA and 21m LiTFSI-PVA gel electrolyte based supercapacitors after 100 cycles.

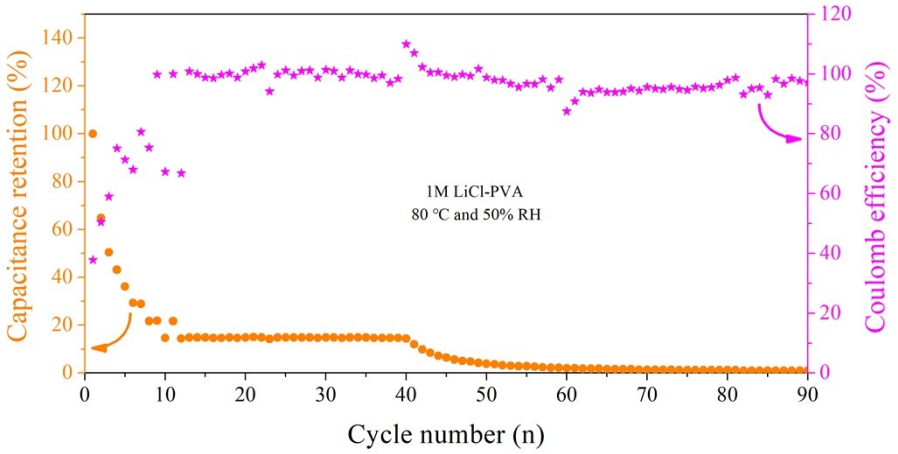

Figure S10. Cycle number dependent cycle performance of 1M LiCl-PVA gel electrolyte based supercapacitors under high temperature (80 ^{o}C-50% RH) condition.

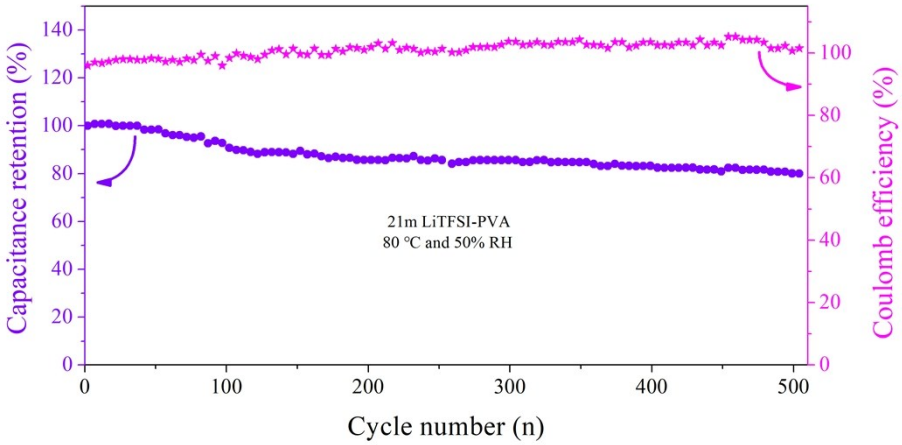

Figure S11. Cycle number dependent cycle performance of 21m LiTFSI-PVA gel electrolyte based supercapacitors under high temperature (80 ^{o}C-50% RH) condition.

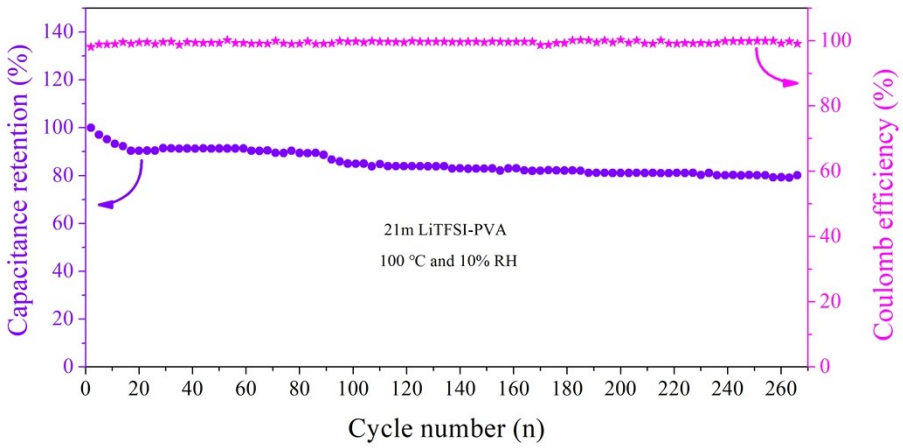

Figure S12. Cycle number dependent cycle performance of 21m LiTFSI-PVA gel electrolyte based supercapacitors under high temperature and ultra-dry (100 °C-10% RH) condition.

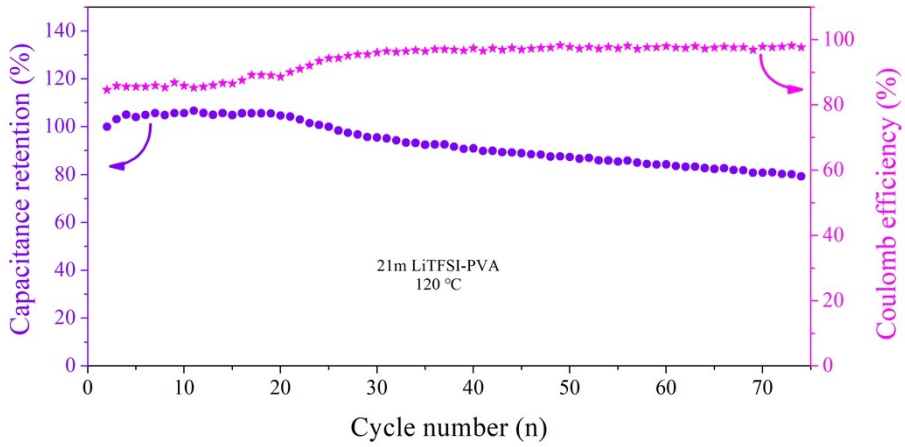

Figure S13. Cycle number dependent cycle performance of 21m LiTFSI-PVA gel electrolyte based supercapacitors under ultra-high temperature (120 °C) condition.

References

[S1] Suo, L.; Borodin, O.; Gao, T.; Olguin, M.; Ho, J.; Fan, X.; Luo, C.; Wang, C.; Xu, K. "Water-in-salt" electrolyte enables high-voltage aqueous lithium-ion chemistries. *Science* **2015,** *350*, 938-43.

[S2] Yamada, Y.; Usui, K.; Sodeyama, K.; Ko, S.; Tateyama, Y.; Yamada, A. Hydrate-melt electrolytes for high-energy-density aqueous batteries. *Nature Energy* **2016,** *1*, 16129.

[S3] Wang, F.; Borodin, O.; Ding, M. S.; Gobet, M.; Vatamanu, J.; Fan, X.; Gao, T.; Eidson, N.; Liang, Y.; Sun, W.; Greenbaum, S.; Xu, K.; Wang, C. Hybrid Aqueous/Non-aqueous Electrolyte for Safe and High-Energy Li-Ion Batteries. *Joule* **2018,** *2*, 927-937.

[S4] Lukatskaya, M. R.; Feldblyum, J. I.; Mackanic, D. G.; Lissel, F.; Michels, D. L.; Cui, Y.; Bao, Z. Concentrated mixed cation acetate "water-in-salt" solutions as green and low-cost high voltage electrolytes for aqueous batteries. *Energy Environ. Sci.* **2018,** *11*, 2876-2883.

[S5] Dou, Q.; Lei, S.; Wang, D.-W.; Zhang, Q.; Xiao, D.; Guo, H.; Wang, A.; Yang, H.; Li, Y.; Shi, S.; Yan, X. Safe and high-rate supercapacitors based on an "acetonitrile/water in salt" hybrid electrolyte. *Energy Environ. Sci.* **2018**, *11*, 3212-3219.

[S6] Dong, Q.; Yao, X.; Zhao, Y.; Qi, M.; Zhang, X.; Sun, H.; He, Y.; Wang, D. Cathodically Stable Li-O 2 Battery Operations Using Water-in-Salt Electrolyte. *Chem* **2018,** *4*, 1345-1358.